



**Universiteit  
Leiden**  
The Netherlands

## **An experimental proposal to study collapse of the wave function in traveling-wave parametric amplifiers**

Reep, T.H.A. van der; Rademaker, L.; Le Large, X.G.A.; Guis, R.H.; Oosterkamp, T.H.

### **Citation**

Reep, T. H. A. van der, Rademaker, L., Le Large, X. G. A., Guis, R. H., & Oosterkamp, T. H. (2020). An experimental proposal to study collapse of the wave function in traveling-wave parametric amplifiers. *Physica Status Solidi B : Basic Research*, 258(4), 2000576.  
doi:10.1002/pssb.202000567

Version: Publisher's Version  
License: [Creative Commons CC BY-NC 4.0 license](#)  
Downloaded from: <https://hdl.handle.net/1887/138755>

**Note:** To cite this publication please use the final published version (if applicable).

# An Experimental Proposal to Study Collapse of the Wave Function in Traveling-Wave Parametric Amplifiers

Thomas H. A. van der Reep, Louk Rademaker, Xavier G. A. Le Large, Ruben H. Guis, and Tjerk H. Oosterkamp\*

The readout of a microwave qubit state occurs using an amplification chain that enlarges the quantum state to a signal detectable with a classical measurement apparatus. However, at what point in this process is the quantum state really “measured”? To investigate whether the “measurement” takes place in the amplification chain, in which a parametric amplifier is often chosen as the first amplifier, it is proposed to construct a microwave interferometer that has such an amplifier added to each of its arms. Feeding the interferometer with single photons, the interference visibility depends on the gain of the amplifiers and whether a measurement collapse has taken place during the amplification process. The visibility as given by standard quantum mechanics is calculated as a function of gain, insertion loss, and temperature. A visibility of  $1/3$  is found in the limit of large gain without considering losses, which is reduced to 0.26 in case the insertion loss of the amplifiers is 2.2 dB at a temperature of 50 mK. It is shown that if the wave function collapses within the interferometer, the measured visibility is reduced compared with its magnitude predicted by standard quantum mechanics once this collapse process sets in.

classical observer. In the case of a PMT, the photon is absorbed in the PMT’s photocathode, and, in turn, a photoelectron is emitted. The electron is multiplied in several stages, resulting in a detectable current pulse at the anode of the device.

A similar situation occurs for microwave photons in quantum bit (qubit) experiments.<sup>[1]</sup> The readout of the qubit state, which can be prepared in a single-photon state,<sup>[2]</sup> occurs via readout lines that run from the device to the measurement apparatus. Implemented in the readout lines is an amplification chain to enlarge the tiny qubit signal to human proportions.

It follows that a measurement can be seen as a process: A quantum signal enters a measurement device (to which we here count the amplification chain in case of qubit experiments), it is amplified, and, finally, the apparatus is read out. In this article, we are interested in the questions:

## 1. Introduction

When a photon hits a single-photon detector, for example, a photomultiplier tube (PMT), a chain of events is set in motion that would lead to an audible click or signal that can be processed by a

at what point in the process did we really “measure” the quantum state? When did the system change from being purely quantum mechanical to classical?

We envision to probe the level of quantum coherence during amplification by building an interferometer around two microwave parametric amplifiers. By comparing the measured interference pattern to the expected interference for a fully quantum-mechanical state, we can infer at which gain level we start deviating from this expectation. In the remainder of this article, we will, therefore, compare interference visibilities for a quantum system to a system that experienced a spontaneous measurement within the interferometer in the Born sense.


The amplifiers we propose to use are typically used in the first amplification stage of qubit readout lines, because they provide a large gain, are nearly quantum-limited, and can be described using conventional quantum theory.<sup>[3–13]</sup> Our experiments are partially inspired by similar setups with optical photons using non-linear optical parametric amplification, by, e.g., Zeilinger and co-workers<sup>[14]</sup> and De Martini and co-workers,<sup>[15]</sup> or other techniques by, e.g., Gisin and co-workers<sup>[16]</sup> and Rempe and co-workers.<sup>[17]</sup>

In this article, we will not argue for one or the other possible mechanisms of the collapse process. The variety of possible ideas is large; see, e.g., the previous review.<sup>[18]</sup> Instead, the work presented here only relies on Born’s rule: the probability of a certain

Dr. T. H. A. van der Reep, X. G. A. Le Large, R. H. Guis,  
Prof. T. H. Oosterkamp  
Leiden Institute of Physics  
Leiden University  
Niels Bohrweg 2, 2333 CA Leiden, The Netherlands  
E-mail: oosterkamp@physics.leidenuniv.nl

Dr. L. Rademaker  
Department of Theoretical Physics  
University of Geneva  
24 quai Ernest-Ansermet, 1211 Geneva, Switzerland

Dr. L. Rademaker  
Perimeter Institute for Theoretical Physics  
Waterloo, Ontario N2L 2Y5, Canada

 The ORCID identification number(s) for the author(s) of this article can be found under <https://doi.org/10.1002/pssb.202000567>.

© 2020 The Authors. Physica Status Solidi B published by Wiley-VCH GmbH. This is an open access article under the terms of the Creative Commons Attribution-NonCommercial License, which permits use, distribution and reproduction in any medium, provided the original work is properly cited and is not used for commercial purposes.

DOI: 10.1002/pssb.202000567

outcome after measurement is proportional to the wave function-squared.

In Section 2, we calculate the Hamiltonian of the interferometer in the lossless case in the time domain. In Section 3, we introduce a measure for the visibility of our interferometer, and we discuss the theoretical predictions for this visibility as a function of the gain of the amplifiers. In Section 4, we discuss the effect of losses followed by our ideas on observing spontaneous collapse in Section 5. In the final section, we conclude by elaborating on the realization of the experiment and estimating the feasibility of the experiment with parametric amplifiers with a gain of 40 dB—a gain commonly used to read out qubits in quantum computation experiments. Some of the detailed calculations are deferred to the appendices.

## 2. Model—Lossless Case

We consider the Mach–Zehnder-type interferometer shown in **Figure 1**. The interferometer is fed by a single-photon source (signal) in input 1, and a traveling-wave parametric amplifier (TWPA) is added to each of its arms. Although other realizations of the experiment are conceivable, we argue in the appendices why we view this version as optimal (see Section A1 and A2). The signal enters a hybrid (the microwave analog of a beam splitter), thereby creating a superposition of 0 and 1 photons in each of the arms. The excitation in the upper arm of the interferometer can be phase shifted, where we assume that the phase shift accounts for an intended phase shift as well as all unwanted phase shifts due to fabrication imperfections and the non-linear phase shift from the TWPA. In the TWPA, amplification takes place by a wave mixing interaction. Throughout this article, we use TWPAs working by a four-wave mixing (4WM) process in a mode, which is phase-preserving (i.e., the amplification is independent of the pump phase). We assume the pump to be degenerate (one signal photon at frequency  $\omega_s$  is created by destroying two pump photons at frequency  $\omega_p$ , and by energy conservation, this gives rise to an idler at frequency  $\omega_i = 2\omega_p - \omega_s$ ). We also assume that the pump is undepleted (we neglect the decrease of pump photons in the amplification process). Finally, we assume that the pump, signal, and idler are phase-matched ( $2k_p = k_s + k_i$ , where  $k$  is the wave number including self-modulation and cross-modulation due to

the non-linear wave mixing). After the TWPA, the excitations from the two arms are brought together using another hybrid, and we can study the output radiation in both the signal and idler mode with detectors A and B.

In this section, we ignore losses, the effect of which we will discuss in Section 4. Under the assumptions introduced earlier<sup>[12,13]</sup>

$$\hat{H}_{\text{TWPA}} = -\hbar\chi(\hat{a}_s^\dagger\hat{a}_i^\dagger + \text{H.c.}) \quad (1)$$

Here,  $\hbar$  is the reduced Planck constant  $h/2\pi$ , and  $\chi$  is the non-linear coupling constant derived from the third-order susceptibility of the transmission line, which considers the pump intensity.  $\hat{a}_n^\dagger$  is the creation operator of mode  $n$ . Using the Heisenberg equations of motion, one can solve for the evolution of the annihilation operators analytically. This yields<sup>[12]</sup>

$$\hat{a}_{s(i)}(t) = \hat{a}_{s(i)}(0) \cosh \kappa + i\hat{a}_{i(s)}^\dagger(0) \sinh \kappa \quad (2)$$

where  $\kappa \equiv \chi\Delta t_{\text{TWPA}}$  is the amplification if the state spends a time  $\Delta t_{\text{TWPA}}$  in the TWPA. Thus, we can determine the average number of photons in the signal (idler) mode as a function of the amplification of the amplifier as

$$\langle \hat{n}_{s(i)} \rangle_{\text{out}} = \langle \hat{n}_{s(i)} \rangle_{\text{in}} \cosh^2 \kappa + (\langle \hat{n}_{i(s)} \rangle_{\text{in}} + 1) \sinh^2 \kappa \quad (3)$$

provided that the signal and/or idler are initially in a number state.  $\langle \hat{n} \rangle_{\text{out(in)}}$  is the average number of photons leaving (entering) the TWPA. From this relation, we define the amplifier gain as  $G_s = \langle \hat{n}_s \rangle_{\text{out}} / \langle \hat{n}_s \rangle_{\text{in}}$ .

Even though, under these assumptions, the calculation can be done analytically (see Section A3), we present the numerical implementation here, because to such an implementation, losses can be added straightforwardly at a later stage.

To numerically obtain the output state, we use QUTIP.<sup>[19]</sup> We first split the Hilbert space of the interferometer into the upper arm and the lower arm. Each of the arm subspaces is additionally divided into a signal and an idler subspace. Hence, our numerical Hilbert space has dimension  $N^4$ , where  $N - 1$  is the maximum amount of signal and idler photons considered in each of the arms. In this framework, the input state is

$$|\psi\rangle = |1\rangle_{\text{up},s} |0\rangle_{\text{up},i} |0\rangle_{\text{low},s} |0\rangle_{\text{low},i} \quad (4)$$

where the labels “up” and “low” refer to the upper and lower arm of the interferometer, respectively. We evolve this state by the time evolution operator, generated by the Hamiltonian  $\hat{H}$  of the system. The first hybrid is described by the Hamiltonian

$$\hat{H}_{\text{h1}} = -\frac{\hbar\pi}{4\Delta t_{\text{h1}}} \left( \sum_{n=s,i} \hat{a}_{\text{up},n}^\dagger \hat{a}_{\text{low},n} + \text{H.c.} \right) \quad (5)$$

where  $\Delta t_{\text{h1}}$  is the time spent in the hybrid. Note that state evolution with the above-mentioned Hamiltonian for a time  $\Delta t_{\text{h1}}$  corresponds to the transformation operator for an ordinary 90° hybrid

$$\hat{U}_{\text{h1}} = e^{i\hat{H}_{\text{h1}}\Delta t_{\text{h1}}/\hbar} = e^{i\frac{\pi}{4} \left( \sum_{n=s,i} \hat{a}_{\text{up},n}^\dagger \hat{a}_{\text{low},n} + \text{H.c.} \right)} \quad (6)$$

By the same reasoning, the Hamiltonian of the phase shifter can be written as

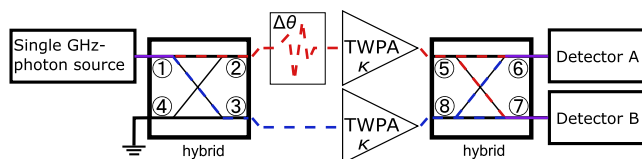


**Figure 1.** Schematic overview of a balanced microwave amplifier setup. Using a 90° hybrid (microwave analog of a beam splitter), a single photon is brought in a superposition, which is then amplified using two identical TWPAs, characterized by an amplification  $\kappa$ . Before entering the TWPAs, the excitation in the upper arm is phase shifted by  $\Delta\theta$ , which is assumed to account for all phase differences within the setup. Using a second 90° hybrid, we can study the output radiation from arms 6 and 7 using detectors A and B. Using 4WM TWPAs, an idler mode is generated. The interference of the idler mode can be studied independently of the interference of the signal mode using the same detectors.

$$\hat{H}_{\text{ps}} = \frac{\hbar\Delta\theta}{\Delta t_{\text{ps}}} \left( \sum_{n=s,i} \hat{a}_{\text{up},n}^\dagger \hat{a}_{\text{up},n} + \text{H.c.} \right) \quad (7)$$

where  $\Delta\theta$  is the applied phase shift. In our numerical calculations, we use

$$\hat{H}_{\text{TWPA}}^{(\text{up/low})} = -\frac{\hbar\kappa(\text{up/low})}{\Delta t_{\text{TWPA}}} (\hat{a}_{(\text{up/low}),s}^\dagger \hat{a}_{(\text{up/low}),i}^\dagger + \text{H.c.}) \quad (8)$$

for the TWPAs. After the TWPAs, the excitations from the two arms are brought together using a second  $90^\circ$  hybrid to create interference, which is measured with detectors A and B. The second hybrid is described by a Hamiltonian  $\hat{H}_{h2}$  similar to Equation (5).

In summary, the proposed theoretical model of the experiment in the absence of losses is as follows. We start with an initial single signal photon in the upper arm, described by Equation (4). We evolve this state for a time  $\Delta t_{h1}$  with Hamiltonian  $\hat{H}_{h1}$ , followed by  $\hat{H}_{\text{ps}}$  for a time  $\Delta t_{\text{ps}}$ , then for a time  $\Delta t_{\text{TWPA}}$  with  $\hat{H}_{\text{TWPA}}$  of Equation (8), and, finally, for a time  $\Delta t_{h2}$  with Hamiltonian  $\hat{H}_{h2}$ . Finally, we will measure the photon densities in detectors A and B, which leads to a given visibility of the interference pattern. For the lossless case, the various  $\Delta t$  values can be chosen arbitrarily.

### 3. Interference Visibility

From the state resulting from our calculations, we get the probability distribution of photon number states in detectors A and B,  $\text{Pr}(n_{A,s} = i, n_{A,i} = j, n_{B,s} = k, n_{B,i} = l)$ , from which we can calculate the photon number statistics and correlations by performing a partial trace (see Section A4). From the photon number statistics, we can compute the visibility of the interference pattern. Although microwave photon counters have been developed in an experimental setting,<sup>[20–22]</sup> we can also envision the measurement of the output radiation using spectrum analyzers. Such instruments measure the output power,  $P$ , of the interferometer as a function of time, and one can determine the number of photons arriving in the detectors as

$$n = \frac{1}{\hbar\omega} \int_{t_1}^{t_2} P(t) dt \quad (9)$$

Measuring the average photon number at detectors A and B, we can define the interference visibility as (Section A5)

$$V_{s(i)} \equiv \frac{\langle n_{B,s(A,i)} \rangle - \langle n_{A,s(B,i)} \rangle}{\langle n_{B,s(A,i)} \rangle + \langle n_{A,s(B,i)} \rangle} \Big|_{\Delta\theta=0} \quad (10)$$

In case the amplifiers have an identical gain, the calculation of the visibility can be simplified by using a smaller Hilbert space. This follows from the following observation: a single TWPA fed with a  $|1\rangle_s|0\rangle_i$  state yields the average number of signal (idler) photons in detector B (A) as calculated with Equation (3). Contrarily, feeding this TWPA with a  $|0\rangle_s|0\rangle_i$  state gives the average number of signal (idler) photons in detector A (B) (see Section A6). This provides a reduced Hilbert space that scales as  $2N^2$  for calculating the visibility. Moreover, this observation implies that the visibility can be computed directly by substituting Equation (3) into (10).

Therefore, the visibility in the lossless case can be solved exactly. Regardless of the input, the parametric amplifier always outputs  $\sinh^2\kappa$  extra photons. In the case of an initial single-photon state, the extra term  $\cosh^2\kappa$  should be added. Consequently, the signal visibility becomes

$$V_s = \frac{\cosh^2\kappa}{\cosh^2\kappa + 2\sinh^2\kappa} \quad (11)$$

In the limit of large gain, the  $\sinh$  and  $\cosh$  become equal in magnitude, and consequently, the visibility tends to  $1/3$ . Similarly, the idler photon number will be  $2\sinh^2\kappa$  in the arm with an initial signal photon and  $\sinh^2\kappa$  in the other; consequently, the idler visibility is constant at  $1/3$ . The reduction from 1 to  $1/3$  is, thus, completely due to the addition of extra photons by the parametric amplifier.

The results of the calculations of the signal and idler visibilities are shown in **Figure 2** (in red) and have been verified using our analytical results from Section A3 up to  $\kappa = 0.8$  and our numerical results up to  $\kappa = 1.7$ . It shows that the signal interference visibility drops from 1 to  $1/3$  with increasing gain, in accordance with the previous study<sup>[23]</sup> and the remarks made above. The signal visibility at  $\kappa = 0$  is 1, because this situation resembles an ordinary single-photon interferometer. The idler visibility at  $\kappa = 0$  is undefined due to the absence of idler photons. Please note that a superposition of zero and one photon before an amplifier with gain  $G$  does not result in a superposition of zero and  $G$  photons after the amplifier. To emphasize that this results in multiphoton interference, we present a figure in Section A4 that shows the photon number correlations within the interferometer arms. Furthermore, this figure shows how many photon Fock states are involved for different gain of the amplifiers.

### 4. The Effect of Losses

To consider the effect of losses (dissipation/insertion loss), we use the Lindblad formalism, which provides the expression for the time evolution of the density matrix,  $\hat{\rho}$ <sup>[24]</sup>

$$\frac{d\hat{\rho}}{dt} = -\frac{i}{\hbar} [\hat{H}, \hat{\rho}] + \sum_{n=1}^{N^2-1} \left( \hat{J}_n \hat{\rho} \hat{J}_n^\dagger - \frac{1}{2} \{ \hat{\rho}, \hat{J}_n^\dagger \hat{J}_n \} \right) \quad (12)$$

where  $\{, \}$  denotes the anticommutator, and  $\hat{J}_n$  are jump operators. These operators describe transitions that the system may undergo due to interactions with the surrounding thermal bath. Losses can be described by the jump operators  $\hat{J}_{\text{out}}$  and  $\hat{J}_{\text{in}}$ .  $\hat{J}_{\text{out}}$  describes a photon leaving the system and entering the bath

$$\hat{J}_{\text{out},n} = \sqrt{\Gamma(1 + n_{\text{th},n})} \hat{a}_n \quad (13)$$

where  $\Gamma$  is the loss rate, and  $n_{\text{th},n} = 1/(\exp(\hbar\omega_n/k_B T) - 1)$  is the thermal occupation number of photons in the bath.  $\hat{J}_{\text{in}}$  describes a photon entering the system from the bath

$$\hat{J}_{\text{in},n} = \sqrt{\Gamma n_{\text{th},n}} \hat{a}_n^\dagger \quad (14)$$

Here, we again see the advantage of using a description in the time domain and putting  $\Delta t$  in the component Hamiltonians (Equations (5), (7), and (8)) in Section 2. The total (specified)

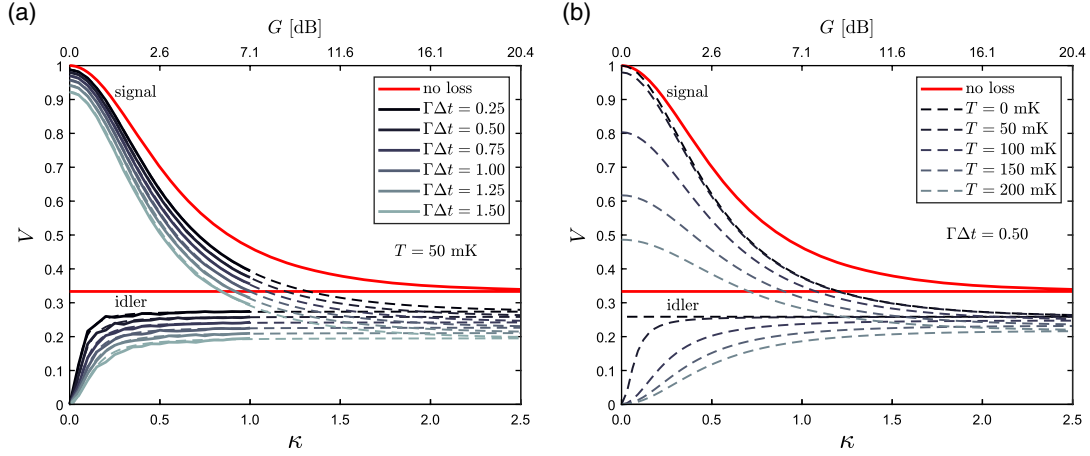


**Figure 2.** Expected visibility of the interference pattern of the interferometer as a function of amplification  $\kappa$  for signal and idler using the reduced Hilbert space (see text). The gain in dB on the upper axis is only indicative and does not consider the losses in the amplifiers ( $G = 10 \log_{10} \langle n_s \rangle_{\text{out}} / \langle n_s \rangle_{\text{in}} = 10 \log_{10} \cosh \kappa + 2 \sinh \kappa$ ). Without loss (red), the visibility tends to 1/3 for large gain. The visibility in case losses are added to the system is plotted in gray for various amounts of loss in the TWPAs at a)  $T = 50 \text{ mK}$  ( $n_{\text{th}} = 8.3 \times 10^{-3}$ ) varying  $\Gamma \Delta t_{\text{TWPA}}$  ( $\Gamma = 100 \text{ MHz}$ , loss  $\approx 4 \Gamma \Delta t$  [dB]) and b)  $\Gamma \Delta t_{\text{TWPA}} = 0.50$  ( $\Gamma = 100 \text{ MHz}$ ) varying  $T$ . For each of the hybrids and the phase shifter, the loss is set to  $\Gamma \Delta t = 0.1$ , and we have set  $\omega_{s,i} = 2\pi \times 5 \text{ GHz}$ . The reduced Hilbert space calculations are presented in continuous lines, whereas an analytical fit and extrapolation according to Equation (16) is dashed. We find that even TWPA losses as high as 6 dB do not reduce the visibility to 0.

loss is mainly determined by the product  $\Gamma \Delta t$  relating to the (insertion) loss as

$$IL = -10 \log_{10} \left( (1 - n_{\text{th},n} / \langle n_{\text{in}} \rangle) e^{-\Gamma \Delta t} + n_{\text{th},n} / \langle n_{\text{in}} \rangle \right) \approx 4 \Gamma \Delta t \quad (15)$$

The approximation holds for  $n_{\text{th},n}$  small. This approach allows us to define a constant loss rate for the whole setup, while adjusting  $\Delta t$  for each component to match the actual loss. As the photon state in the interferometer is now described by a density matrix, the amount of memory for these calculations scales as  $N^8$ .

To study the effect, we set  $\omega_{s,i} = 2\pi \times 5 \text{ GHz}$  for now. This implies  $n_{\text{th},n}$  as used in Equations (13), (14), and (15) can be set to a constant  $n_{\text{th}}$ . The loss rate  $\Gamma$  is set to 100 MHz for the full setup. For the hybrids and the phase shifter, we choose  $\Delta t_{(h_1, ps, h_2)} = 1 \text{ ns}$  ( $IL \approx 0.4 \text{ dB}$ ) and study the effect of losses in the TWPAs by varying  $\Delta t_{\text{TWPA}}$  and  $T$ . We evolve the state under the Hamiltonians  $\hat{H}_{h_1} \rightarrow \hat{H}_{ps} \rightarrow \hat{H}_{\text{TWPA}}^{(\text{up/low})} \rightarrow \hat{H}_{h_2}$  as described in Section 2.

Unfortunately, running the numeric calculation, we were not able to increase the amplification to  $\kappa > 0.6$  due to QUTIP working with a version of SciPy supporting only int32 for element indexing. However, again, it appears that we can use the method of the reduced Hilbert space sketched in the last section. Thus, the problem only scales as  $2N^4$ , and we have performed the numeric calculation up to  $\kappa = 1.0$ .

Applying the reduced Hilbert space approach, we found that the parametric amplifier's output in the presence of losses can be fitted according to

$$\langle \hat{n}_{s(i)} \rangle_{\text{out}} = \langle \hat{n}_{s(i)} \rangle_{\text{out}}|_{\kappa=0} \cosh^2 \kappa + (\langle \hat{n}_{s(i)} \rangle_{\text{out}}|_{\kappa=0} + 1) e^{-f} \sinh^2 \kappa \quad (16)$$

where the parameter  $f$  depends on  $\Gamma$ , the various  $\Delta t$  values (if  $T > 0$ ),  $n_{\text{th}}$ , and the input state and is determined by a fit

to the numerical data (see Section A7).  $\langle \hat{n}_{s(i)} \rangle_{\text{out}}|_{\kappa=0}$  is the number of photons leaving the amplifier in case no amplification is present

$$\langle \hat{n}_{s(i)} \rangle_{\text{out}}|_{\kappa=0} = (\langle \hat{n}_{s(i)} \rangle_{\text{in}} - n_{\text{th}}) e^{-\Gamma \Delta t_{\text{tot}}} + n_{\text{th}} \quad (17)$$

This allows us to extrapolate the results to higher gain.

The results of the calculations with loss are also shown in Figure 2, assuming the full setup is at a constant temperature. We observe that losses decrease the interference visibility with respect to the case where losses were neglected. However, even for TWPA losses as high as 6 dB, the interference visibility survives.

As in the no-loss case, the signal and idler visibility converge asymptotically to the same value. In the high-gain limit, the interference visibility is given by

$$V_{s,i} = (1 + 2e^{\Gamma \Delta t_{\text{tot}} - f} + 2n_{\text{th}} e^{\Gamma \Delta t_{\text{tot}}} (1 + e^{-f}) (1 - e^{-\Gamma \Delta t_{\text{tot}}}))^{-1} \quad (18)$$

by Equation (16). Assuming  $n_{\text{th}} \ll 1$ , we find  $f \approx \Gamma \Delta t_{\text{tot}} / 2$  (see Section A7), and as a result

$$V_{s,i} \approx \frac{1}{1 + 2e^{\Gamma \Delta t_{\text{tot}} / 2}} \quad (19)$$

Thus, in the limit of low temperature, we find that the interference disappears exponentially with the loss in the setup. The visibility becomes 1/e times the lossless visibility at  $\Gamma \Delta t_{\text{tot}} = 3$  ( $IL \approx 12 \text{ dB}$ , but at this loss, it will not be possible to keep the amplifiers in the limit of low  $n_{\text{th}}$ ).

Contrarily, in the limit of low losses, we find that  $f \approx 0$  and

$$V_{s,i} \approx \frac{1}{3 + 4n_{\text{th}} \Gamma \Delta t_{\text{tot}}} \quad (20)$$

Thus, we see that the interference visibility becomes 1/e times the lossless visibility when approximately one photon jumps from the bath into the system.

Experimentally, the conclusion is that efforts need to be made to make the losses in the parametric amplifier so small that the amplifier remains cold.

## 5. Observing Collapse

Although there is currently no universally agreed-upon model that describes state collapse, we propose to mathematically investigate the effect of collapse on the proposed experiment using Born's rule in the following way.

To model the collapse, we split each of the amplifiers in the upper and lower arm of the interferometer in two parts, and we assume that the collapse takes place instantaneously in between these two parts; see **Figure 3**. Thus, the first part of each amplifier can be characterized by an amplification  $\eta\kappa$  and the second by an amplification  $(1-\eta)\kappa$ , where  $\eta \in [0, 1]$  sets the collapse position. If  $\eta = 0$ , the collapse takes place between the first hybrid and the amplifiers, whereas for  $\eta = 1$ , the collapse takes place between the amplifiers and the second hybrid. For  $0 < \eta < 1$ , the collapse takes place within the amplifiers. For simplicity, we ignore the fact that a photon is a spatially extended object. Moreover, we will ignore here that the collapse process might be expected to be stochastic in its position  $\eta$ , a point we will return to in Section 6.

Then, by Born's rule, we have to assume a collapse phenomenology. Regardless of the precise mechanism, such a collapse will destroy the entanglement between the two interferometer arms and yield a classical state. As for the type of classical state, we will consider two options: the state collapses onto 1) a number state, or 2) onto a coherent state. For both these options, we will study the effect on the interference visibility given in the following.

### 5.1. Collapse Onto a Number State

In case the collapse projects the instantaneous state onto a number state, the state after projection is given by  $|\psi_{\text{coll}}\rangle(N, M) = |N+1\rangle_{\text{up},s}|N\rangle_{\text{up},i}|M\rangle_{\text{low},s}|M\rangle_{\text{low},i}$  or  $|\psi_{\text{coll}}\rangle(N, M) = |N\rangle_{\text{up},s}|N\rangle_{\text{up},i}|M+1\rangle_{\text{low},s}|M\rangle_{\text{low},i}$ , depending on whether the initial photon went through the upper or lower arm of the interferometer. Hence, this collapse phenomenology can be thought of as resulting from the collapse taking place as a consequence of a which-path detection within the amplifiers, which could happen in a power meter that measures the intensity (energy) of an incoming signal. The second part of the amplifiers, characterized by the amplification  $(1-\eta)\kappa$ , evolves  $|\psi_{\text{coll}}\rangle$  to

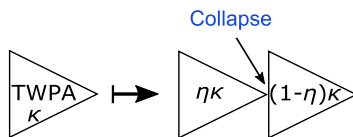


**Figure 3.** Model of a TWPA in which a quantum state collapse takes place. The quantum TWPA, characterized by amplification  $\kappa$ , is split into two parts. One is characterized by the amplification  $\eta\kappa$  and the other by  $(1-\eta)\kappa$ , where  $\eta \in [0, 1]$  determines the position of the collapse. We assume that the state collapse takes place instantaneously between the two parts of the amplifier.

$|\psi'_{\text{coll}}\rangle = \sum_{N,M} c_{NM} |\psi_{\text{coll}}\rangle(N, M)$ , where  $c_{NM}$  are the weights determined by  $(1-\eta)\kappa$  and  $\sum_{N,M} |c_{NM}|^2 = 1$ .  $|\psi'_{\text{coll}}\rangle$  is the state just before the second hybrid.

To determine the effect on the interference visibility of such a collapse, we calculate  $\langle n_{X,n} \rangle = \hat{a}_{X,n}^\dagger \hat{a}_{X,n}$ , the number of photons arriving in detector  $X \in \{A, B\}$  in mode  $n \in \{s, i\}$ . This equation can be rewritten in terms of creation and annihilation operators of the upper and lower arm of the interferometer by the standard hybrid transformation relations  $\hat{a}_{\{A\}\{B\},n} \mapsto (\{1\}[i]\hat{a}_{\text{up},n} + \{i\}[1]\hat{a}_{\text{low},n})/\sqrt{2}$  to find

$$V_n^{\text{coll}} = \frac{i\langle \hat{a}_{\text{up},n}^\dagger \hat{a}_{\text{low},n} - \hat{a}_{\text{up},n} \hat{a}_{\text{low},n}^\dagger \rangle}{\langle \hat{a}_{\text{up},n}^\dagger \hat{a}_{\text{up},n} + \hat{a}_{\text{low},n}^\dagger \hat{a}_{\text{low},n} \rangle} \quad (21)$$

which equals 0 for any  $|\psi'_{\text{coll}}\rangle$ . Hence, we find that a collapse onto a number state within the interferometer causes a total loss of interference visibility.

### 5.2. Collapse onto a Coherent State

If a collapse in the amplifiers projects the quantum state onto a coherent state, the state after collapse is  $|\psi_{\text{coll}}\rangle = |\alpha_{\text{up},s}\rangle|\alpha_{\text{up},i}\rangle|\alpha_{\text{low},s}\rangle|\alpha_{\text{low},i}\rangle$  with overlap  $c_{\text{coll}} = \langle \psi_{\text{coll}} | \psi_q \rangle$ . Here  $|\psi_q\rangle$  is the instantaneous quantum state at the moment of collapse. This collapse phenomenology can be thought of as a collapse of the electrons in the transmission lines connecting the different parts of the interferometer onto position states characterized by a well-defined phase and amplitude. This is in contrast to the electrons' ill-defined phase and amplitude in case the transmission lines are excited with a (superposition of) photonic number states. Moreover, the coherent state is generally seen as the most classical state in quantum mechanics. Such a collapse might occur in a vector network analyzer, which measures both the intensity as well as the phase of an incoming signal.

In this case, the second part of the parametric amplifiers characterized by  $(1-\eta)\kappa$  evolves the amplitudes  $\alpha$  in  $|\psi_{\text{coll}}\rangle$  into average amplitudes

$$\bar{\alpha}_{\text{up(low)},s(i)} = \alpha_{\text{up(low)},s(i)} \cosh(1-\eta)\kappa + i\alpha_{\text{up(low)},i(s)}^* \sinh(1-\eta)\kappa \quad (22)$$

by Equation (2). Then, the number of photons arriving in each detector, for each individual collapse, is

$$n_{A(B),n}^{\text{coll}} = \frac{1}{2} (|\bar{\alpha}_{\text{up},n}|^2 + |\bar{\alpha}_{\text{low},n}|^2 \mp 2|\bar{\alpha}_{\text{up},n}||\bar{\alpha}_{\text{low},n}|\sin(\phi_{\text{low},n} - \phi_{\text{up},n})) \quad (23)$$

where  $\phi_i$  is the phase of the state  $\bar{\alpha}_i$ . Thus, we can obtain the average number of photons arriving in each detector as an integration over all possible collapsed states weighed by their probability. That is

$$\langle n_{X,n}^{\text{coll}} \rangle = \frac{1}{\pi^4} \int n_{X,n}^{\text{coll}} |c_{\text{coll}}|^2 d^2\alpha_{\text{up},s} d^2\alpha_{\text{up},i} d^2\alpha_{\text{low},s} d^2\alpha_{\text{low},i} \quad (24)$$

in which  $d^2\alpha_n$  denotes the integration over the complex amplitude of the coherent state  $n$ . Then, we determine the interference visibility according to Equation (10).

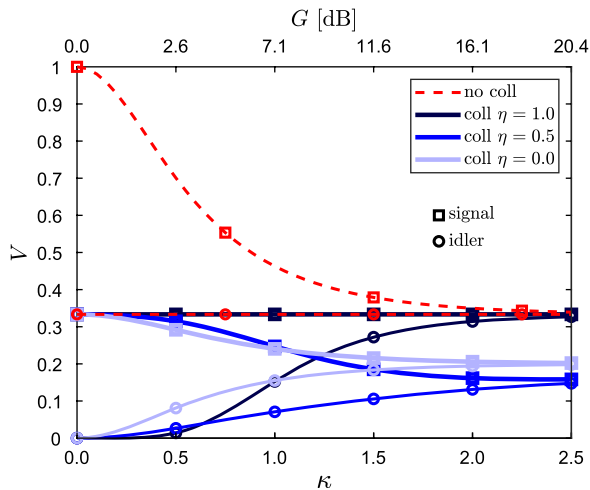


**Figure 4.** Comparison of the interference visibility resulting from a full quantum calculation without collapse and under the assumption of state collapse to coherent states within the interferometer assuming no losses. If the state collapses between the amplifiers and the second hybrid ( $\eta = 1$ ), the visibility is  $1/3$  for the signal and rises to  $1/3$  with increasing amplification for the idler. In case the collapse takes place halfway through the amplifiers ( $\eta = 0.5$ ), the visibility tends to  $0.15$  for both signal and idler for high gain, and if the collapse is between the first hybrid and the amplifiers ( $\eta = 0$ ), the visibility goes to  $0.2$  for signal and idler.

In case we assume that the interferometer is lossless, we can perform such a calculation analytically (see Section A8). The resulting interference visibility is plotted in **Figure 4** in which we can observe that the interference visibility at high gain depends on the location of collapse. For  $\eta = 1$ , the signal and idler visibility equals  $1/3$ . For  $\eta = 0.5$ , both visibilities tend to  $\approx 0.15$ , and in case  $\eta = 0$ , the visibility tends to  $1/5$  for both signal and idler.

## 6. Experimental Realization and Feasibility

As a single-photon source, we propose to use a qubit capacitively coupled to a microwave resonator.<sup>[2]</sup> For the amplifiers, we can use TWPAs in which the non-linearity is provided by Josephson junctions. Currently, TWPAs providing 20 dB ( $\kappa = 2.5$ ) of gain and 2 dB of (insertion) loss that operate at  $T = 30$  mK have been developed.<sup>[9]</sup>

The amplification process within the TWPAs is driven by a coherent pump signal. Instead of increasing the gain of the TWPAs by increasing the pump power, we propose to vary the amplification by varying the pump frequency. In the latter method, the amplification varies due to phase-matching conditions within the amplifier. The advantage is that in this manner, the transmission and reflection coefficients of the TWPA, which depend on the pump power,<sup>[25]</sup> can be kept constant while varying the gain in the interferometer. Although we assumed perfect phase matching in the amplifiers for the results shown in this article, we do not expect a large difference if one changes from a varying pump-power approach to a varying phase-matching approach.

Our calculations are based on a Taylor expansion up to the third-order susceptibility of a parametric amplifier. Typically, microwave TWPAs work close to the critical current of the device, such that this assumption might break down and we need to consider higher orders as well. For TWPAs based on Josephson junctions, we can estimate as follows at which current a higher order Taylor expansion would become necessary.

In the Hamiltonian of a TWPA with Josephson junctions, the non-linearity providing wave mixing arises from the Josephson energy

$$E_J = I_c \varphi_0 \left( 1 - \cos\left(\frac{\Phi}{\varphi_0}\right) \right) = I_c \varphi_0 \sum_{n=1}^{\infty} \frac{(-1)^{n-1}}{(2n)!} \left(\frac{\Phi}{\varphi_0}\right)^{2n} \quad (25)$$

Here,  $I_c$  is the junction's critical current, and  $\varphi_0$  is the reduced flux quantum  $\Phi_0/2\pi$ . Hence, the second-order ( $n = 3$ ) non-linear effects have a factor  $4!(\Phi_p/\varphi_0)^2/6!$  smaller contribution than the first-order non-linear effects. This contribution causes the generation of secondary idlers and additional modulation effects. If we require that this contribution is less than 5% of the energy contribution of the first-order non-linear terms, we can estimate that the theory breaks down at  $\Phi_p/\varphi_0 \approx 1.2$  ( $I_p/I_c \approx 0.78$ ). It is only in the third-order non-linearity that terms proportional to  $(\hat{a}_s^\dagger \hat{a}_i^\dagger)^n$  with  $n > 1$  start to appear, apart from yet additional secondary idlers and further modulation effects. These terms have a maximal contribution of approximately a factor  $4!(\Phi_p/\varphi_0)^4/8! \approx 4 \times 10^{-3}$  less than the first-order non-linear term at the critical flux ( $\Phi_p/\varphi_0 = \pi/2$ ) and are, therefore, negligible for practical purposes.

The other assumption that might break down is the assumption of an undepleted pump. If the signal power becomes too close to the pump power, the pump becomes depleted. Typically, this happens at  $P_s \approx P_p/100$ .<sup>[25]</sup> At  $I_p/I_c = 0.9$ ,  $P_p \approx 1$  nW in a  $50 \Omega$ -transmission line with  $I_c = 5 \mu\text{A}$ . In case our qubit photon source has a  $T_1$  time of  $\approx 100$  ns,<sup>[2]</sup> implying the photon has a duration in that order, the number of 5 GHz-pump photons available for amplification is in the order of  $10^7$ . Hence, we expect that pump depletion only starts to play a significant role in case the gain becomes about 50 dB.

In our calculations, the only loss effect that was not considered was the loss of pump photons due to the insertion loss of the TWPA. If the insertion loss amounts to 3 dB, half of the pump photons entering the device will be dissipated. To the best of our knowledge, this effect has not been considered in the literature. However, effectively, this must lead to a coupling constant  $\chi$  (Equation (1)), which decreases in magnitude in time. In a more involved calculation, this effect needs to be considered for a better prediction of the experimental outcome of the visibility.

Apart from making  $\chi$  time-dependent, the loss of pump photons will be the main reason for an increase in the temperature of the amplifiers. A dilution refrigerator is typically able to reach temperatures of 10 mK with a cooling power of  $1 \mu\text{W}$ . However, the heat conductivity of the transmission line to the cold plate of the refrigerator will limit the temperature of the TWPA. Still, we estimate that a dissipation in the order of  $0.5$  nW will not heat up the amplifiers above 50 mK. However, as shown in Figure 2, even if the amplifiers heat up to temperatures as high as 200 mK, we still expect a visibility that should be easily measurable, if no collapse would occur.

Finally, a more accurate calculation of the expected interference visibility would need to consider reflections within the setup as well as the possible difference in gain between both amplifiers and decoherence mechanisms that might be present, and we have not considered here, such as pure dephasing.

The results we obtained for the interference visibility with a collapse within the interferometer are only speculative as the mechanism of state collapse is currently not understood. In case the state collapses onto a number state, the resulting interference visibility is 0 for any gain. We anticipate that this number might increase in case the losses are considered in the calculation; however, still, we expect that the difference in interference visibility between the cases of no collapse and collapse within the interferometer should be easily detectable.

Contrarily, if the state collapses onto a coherent state, the visibility depends on the location of the collapse. This result should be interpreted as follows. Let us assume that the state collapses at a gain of 20 dB ( $\kappa = 2.5$ ). Then, neglecting losses, the predicted signal interference visibility is  $\approx 1/3$  in case the state does not collapse, whereas it equals  $1/3$  in the case the state collapses between the amplifiers and the second hybrid ( $\eta = 1$ ). However, if we increase the gain further, the expected location of collapse (the location at which the state is amplified by 20 dB) moves toward the first hybrid ( $\eta < 1$ ), which will become apparent in the measurement result as an initial gradual drop in the interference visibility followed by an increase; see Figure 4. Simultaneously, the idler visibility is expected to show the same behavior.

It should be noted that the result for a calculation, in which one assumes a state collapse onto a coherent state between the interferometer and the detectors, is the same as when the state would collapse between the amplifiers and the second hybrid of the interferometer. However, even if this would be the case, one can observe a collapse within the interferometer if the collapse takes place within the amplifiers.

A second remark to this collapse phenomenology is that it does not conserve energy. If one considers some state  $|\psi\rangle$  with an average photon number  $n$ , one finds that a collapse onto a coherent state adds one noise photon to the state, i.e.,  $\langle n \rangle \mapsto \langle n \rangle^{\text{coll}} = n + 1$ . This behavior holds for each of the Hilbert subspaces. Such an increase in energy is a property of many spontaneous collapse models.<sup>[26–30]</sup>

It is due to this added photon and its amplification (see Equation (22)) in the classical part of the TWPAs that the differences in the predicted interference visibility with and without state collapse arise, although in the collapse, the phase correlations between the signal and idler modes in both arms are preserved. The latter can be observed in our expression for  $c_{\text{coll}}$  in Section A8. In case the photon is added after the amplifiers ( $\eta = 1$ ), this photon can be added directly to the expression for the number of output photons (Equation (3)), such that the expression for the interference visibility (Equation (10)) goes from  $V_s = \cosh^2\kappa / (\cosh^2\kappa + 2\sinh^2\kappa)$  to  $V_s^{\text{coll}} = \cosh^2\kappa / (\cosh^2\kappa + 2\sinh^2\kappa + 2) = 1/3$  using the reduced Hilbert space approach. In case the state collapses before the amplifiers ( $\eta = 0$ ), this photon can be added to  $\langle \hat{n}_{s(i)} \rangle$  in Equation (3) directly. Then, as the amplifiers are, in this case, fully classical, one can drop the +1 in the term  $(\langle \hat{n}_{s(i)} \rangle + 1)$  in this equation, which results from the commutator  $[\hat{a}, \hat{a}^\dagger] = 1$ . As such, it is

found that the interference visibility reduces to  $V_s^{\text{coll}} = \cosh^2\kappa / (3\cosh^2\kappa + 2\sinh^2\kappa)$ , which equals  $1/5$  in the high-gain limit.

In case one assumes a collapse onto a coherent state, one could calculate the expected interference visibility in case the losses are included numerically by calculating the overlap between the state evolved until collapse and many (order  $10^6$ ) randomly chosen coherent states. However, due to the issue with SciPy noted in Section 4, we could not perform this calculation for a reasonable number of photons. Still, we expect that, although the difference in visibility between the situations with and without collapse in the interferometer might be decreased, this difference is measurable.

Finally, as remarked in Section 5, it might be expected that the collapse will take place at a position  $\eta$ , which is stochastic in nature. In principle, this can be considered as

$$\langle n_{X,n,\text{exp}}^{\text{coll}} \rangle = \int_0^1 \text{PDF}(\eta) \langle n_{X,n}^{\text{coll}}(\eta) \rangle d\eta + \left( 1 - \int_0^1 \text{PDF}(\eta) d\eta \right) \langle n_{X,n}^q \rangle \quad (26)$$

where  $\langle n_{X,n,\text{exp}}^{\text{coll}} \rangle$  is the experimentally expected number of photons in detector X and mode  $n$  including a stochastic state collapse,  $\langle n_{X,n}^{\text{coll}}(\eta) \rangle$  corresponds to the number of photons after collapse calculated in Section 5, and  $\langle n_{X,n}^q \rangle$  is the number of photons expected from quantum evolution of the system as calculated in Section 3. PDF( $\eta$ ) is the probability density function for  $\eta$  normalized to the probability that the collapse occurs in the interferometer. From these average photon numbers, the visibility can be calculated using Equation (10). In case of a number state collapse, the contribution to the interference visibility after a collapse equals 0; see Section 5, and the visibility will decrease according to the probability that the collapse occurs in the interferometer. On the other hand, for a coherent state collapse, the visibility after collapse is unequal to 0, and thus, we would need an explicit model for the stochasticity of the collapse process. Although we have not performed the calculation for a coherent state collapse, we may still expect the same behavior as described before, i.e., as soon as the collapse process sets in the interference visibility decreases faster to  $1/3$  than expected from our calculations presented in Section 3, after which the visibility will decrease to  $1/5$ , while increasing the gain of both amplifiers further.

Under these considerations, an experiment with two 40 dB amplifiers ( $\kappa = 4.7$ ) at 50 mK, which might be developed if losses are reduced, is feasible.

## 7. Conclusion

We conclude that it should be possible to determine whether or not a 40 dB-microwave parametric amplifier causes a wave function to collapse. If we insert such an amplifier into each of the two arms of an interferometer, we can measure the visibility of the output radiation. Neglecting losses, the interference visibility of both signal and idler tends to  $1/3$  with increasing gain, in case no collapse takes place. If the state collapses onto a number state within the interferometer, the visibility reduces to 0, whereas we found a significant deviation from  $1/3$  in the case that the



state collapses onto a coherent state. In case the insertion loss of the amplifiers is 2.2 dB, while the temperature of the devices is 50 mK, we estimate an interference visibility of 0.26 at large amplifier gain. In case wave function collapse sets in, we still expect the visibility to decrease measurably.

In summary, this article predicts the possible outcome for an experiment. If projection operators are at work in parametric amplifiers in the same way that they appear to be at work in clicking single-photon detectors, this article predicts they might be detectable.

## Appendix

### A1. Experimental Realization Using Resonator-Based Parametric Amplifiers

The discussed setup is not the only conceivable realization of the experiment. Instead of using a TWPA, it is also possible to use a resonator-based parametric amplifier, such as the Josephson parametric amplifier (JPA), if the bandwidth of the photons is smaller than the bandwidth of the amplifier. TPWAs are broadband ( $BW \approx 5 \text{ GHz}^{[9]}$ ), whereas JPAs are intrinsically limited in their bandwidth ( $BW \approx 10 \text{ MHz}^{[3]}$ ). However, both amplifiers are suitable to amplify a single photon with a 1 MHz bandwidth, in case our photon source would have a  $T_1$  time in excess of 1  $\mu\text{s}$ .

As we want to minimize losses and reflections in the interferometer arms, using a TWPA leads to a Mach–Zehnder-type interferometer, whereas using a JPA results in a Michelson-type interferometer; see **Figure 5**. In case the JPA works in the non-degenerate regime ( $\omega_s \neq \omega_i$ ), the results of the interference visibility as presented in this article are the same.

### A2. Non-Degenerate Versus Degenerate Amplifiers

In the main text, we considered the amplifiers to be non-degenerate, i.e.,  $\omega_s \neq \omega_i$ . In case the amplifiers work in a degenerate regime

$$\hat{H}_{\text{deg}} = -\hbar\chi(\hat{a}_s^\dagger \hat{a}_s^\dagger e^{i\Delta\phi} + \text{H.c.}) \quad (27)$$

and the amplification will be dependent on the relative phase,  $\Delta\phi$ , between the signal and the pump; see **Figure 6**. In this case, we can still measure a visibility—in fact,  $\Delta\phi$  can be used as a phase shifter in the experiment—as shown in **Figure 7**. In this figure, the expected interference visibility in case the quantum

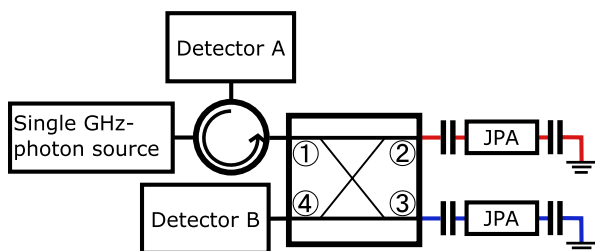


**Figure 5.** Schematic overview of the implementation of the experiment using JPAs. In this case, it is beneficial to use a Michelson-type interferometer to minimize losses.

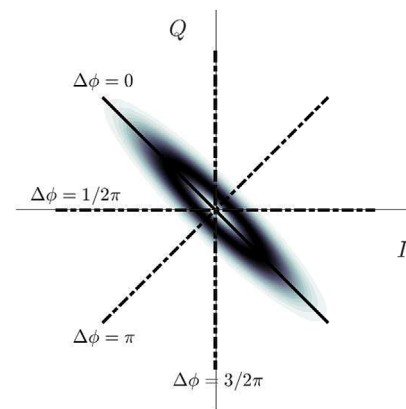


**Figure 6.** Wigner function of the state entering the hybrid after amplification by a degenerate amplifier (Equation (27)). Shown is the case where the signal and the pump are in phase ( $\Delta\phi = 0$ ). If  $\Delta\phi \neq 0$ , the Wigner function rotates according to the dashed-dotted lines.

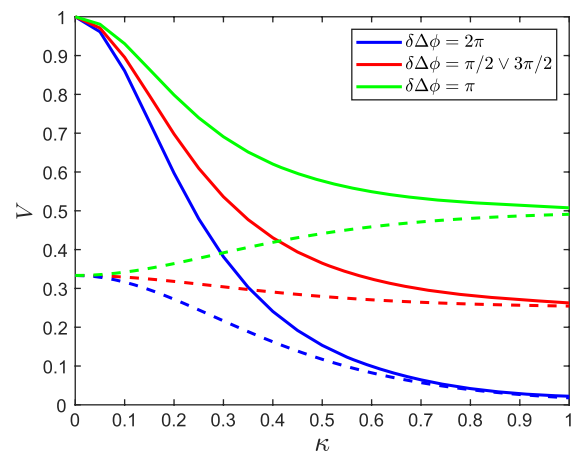


**Figure 7.** Interference visibility of the experiment implementing degenerate parametric amplifiers as a function of amplification  $\kappa = \chi\Delta t_{\text{deg}}$  and the difference in relative phase of the two amplifiers,  $\delta\Delta\phi = \Delta\phi_{\text{up}} - \Delta\phi_{\text{low}}$ .  $\delta\Delta\phi$  can effectively be used as a phase shifter, and we assume the interferometer to be lossless. The continuous lines represent the visibility resulting from a quantum calculation. The dashed lines result from a calculation in which we assume state collapse into coherent states between the amplifiers and the second hybrid ( $\eta = 1$ ; see Section 5 and Section A8).

state does not collapse within the interferometer is depicted using continuous lines. In case we assume that the state collapses into a coherent state in between the amplifiers and the second hybrid, the resulting visibility can be calculated using the method outlined in Section 5 and A8. The result is shown in **Figure 7** using dashed lines. It is observed that for large amplification  $\kappa$ , the two results approach each other asymptotically.

The main advantage of using non-degenerate instead of degenerate amplifiers is that the latter have not been developed. In the microwave regime, parametric amplifiers have been developed using Josephson junctions and kinetic inductance as the source of non-linear wave mixing and the resulting amplification. Both these sources lead naturally to non-degenerate devices as the non-linearity scales quadratically with pump current.

One can use these as quasi-degenerate amplifiers by, e.g., biasing the device using a direct current. This complicates the setups as proposed in Figure 1 and 5, which can be a source of reflections and decoherence. Moreover, such amplifiers will always have non-degenerate contributions to their amplification, which complicates the analysis of the experiment. Third, non-degenerate amplifiers enable one to study two interference visibilities (of both signal and idler) instead of one. For these reasons, we consider non-degenerate amplifiers to be more suited for our proposed experiment.

### A3. Analytical Model

Without losses and using the assumptions for the TWPAs as presented in Section 3, we can obtain an analytical expression for the output state. We start by creating a single signal photon in input channel 1.

$$|\psi\rangle_1 = \hat{a}_{1s}^\dagger |0_{1s}, 0_{1i}, 0_{4s}, 0_{4i}\rangle = |1_{1s}, 0_{1i}, 0_{4s}, 0_{4i}\rangle \quad (28)$$

Here,  $\hat{a}^\dagger$  is the creation operator working on the vacuum. We then incorporate the  $90^\circ$  hybrid by making the transformation

$$\hat{a}_{1s}^\dagger \mapsto \frac{1}{\sqrt{2}} (\hat{a}_{2s}^\dagger + \hat{a}_{3s}^\dagger) \quad (29)$$

Next, a phase shift  $\Delta\theta$  is applied to the upper arm

$$\hat{a}_{2s}^\dagger \mapsto \hat{a}_{2s}^\dagger e^{i\theta\hat{a}_{2s}^\dagger\hat{a}_{2s}} \quad (30)$$

at which the state just before the TWPAs is

$$|\psi\rangle_3 = \frac{1}{\sqrt{2}} \left[ \cosh^{-2}\kappa \cosh^{-1}\kappa' e^{i\Delta\theta} \sum_{n,m=0}^{\infty} \frac{i^n \tanh^n \kappa}{n!} \frac{i^m \tanh^m \kappa'}{m!} (\hat{a}_{5s}^\dagger \hat{a}_{5i}^\dagger)^n (\hat{a}_{8s}^\dagger \hat{a}_{8i}^\dagger)^m \hat{a}_{5s}^\dagger \right. \\ \left. + \cosh^{-1}\kappa \cosh^{-2}\kappa' \sum_{n,m=0}^{\infty} \frac{i^n \tanh^n \kappa}{n!} \frac{i^m \tanh^m \kappa'}{m!} (\hat{a}_{5s}^\dagger \hat{a}_{5i}^\dagger)^n (\hat{a}_{8s}^\dagger \hat{a}_{8i}^\dagger)^m \hat{a}_{8s}^\dagger \right] \cdot |0_{5s}, 0_{5i}, 0_{8s}, 0_{8i}\rangle \quad (36)$$

where  $\kappa$  and  $\kappa'$  are the amplification in the upper arm and lower arm, respectively. Finally, the state traverses the second hybrid, which is modeled by the transformations

$$\hat{a}_5^\dagger \mapsto \frac{1}{\sqrt{2}} (\hat{a}_6^\dagger + \hat{a}_7^\dagger) \\ \hat{a}_8^\dagger \mapsto \frac{1}{\sqrt{2}} (\hat{a}_6^\dagger + i\hat{a}_7^\dagger) \quad (37)$$

for both signal and idler. Thus, we arrive at the output state

$$|\psi\rangle_4 = \frac{1}{2} \cosh^{-1}\kappa \cosh^{-1}\kappa' \left[ \left( \frac{-e^{i\Delta\theta}}{\cosh \kappa} + \frac{1}{\cosh \kappa'} \right) \hat{a}_{6s}^\dagger + \left( \frac{ie^{i\Delta\theta}}{\cosh \kappa} + \frac{i}{\cosh \kappa'} \right) \hat{a}_{7s}^\dagger \right] \\ \cdot \sum_{n,m=0}^{\infty} \frac{i^n \tanh^n \kappa}{2^n n!} \frac{i^m \tanh^m \kappa'}{2^m m!} (-\hat{a}_{6s}^\dagger \hat{a}_{6i}^\dagger + i\{\hat{a}_{6s}^\dagger \hat{a}_{7i}^\dagger + \hat{a}_{7s}^\dagger \hat{a}_{6i}^\dagger\} + \hat{a}_{7s}^\dagger \hat{a}_{7i}^\dagger)^n (\hat{a}_{6s}^\dagger \hat{a}_{6i}^\dagger + i\{\hat{a}_{6s}^\dagger \hat{a}_{7i}^\dagger + \hat{a}_{7s}^\dagger \hat{a}_{6i}^\dagger\} - \hat{a}_{7s}^\dagger \hat{a}_{7i}^\dagger)^m |0_{6s}, 0_{6i}, 0_{7s}, 0_{7i}\rangle \quad (38)$$

$$|\psi\rangle_2 = \frac{1}{\sqrt{2}} (ie^{i\Delta\theta} \hat{a}_{2s}^\dagger \hat{a}_{2s}^\dagger + \hat{a}_{3s}^\dagger) |0_{2s}, 0_{2i}, 0_{3s}, 0_{3i}\rangle \quad (31)$$

$$= \frac{1}{\sqrt{2}} (ie^{i\Delta\theta} |1_{2s}, 0_{2i}, 0_{3s}, 0_{3i}\rangle + |0_{2s}, 0_{2i}, 1_{3s}, 0_{3i}\rangle) \quad (32)$$

For the TWPAs, we use the following Hamiltonian in the interaction picture

$$\hat{H}_{\text{TWPA}}^{\text{eff}} = -\hbar\chi (\hat{a}_s^\dagger \hat{a}_i^\dagger + \hat{a}_s \hat{a}_i) \quad (33)$$

Evolving the state under this Hamiltonian as  $|\psi\rangle_3 = e^{-i\hat{H}_{\text{TWPA}}^{\text{eff}} t/\hbar}$ , the output for a single amplifier in a single arm is<sup>[31]</sup>

$$e^{-i\hat{H}_{\text{TWPA}}^{\text{eff}} t/\hbar} |N_s, 0_i\rangle = \cosh^{-(1+N_s)\kappa} \sum_{n=0}^{\infty} \frac{(i \tanh \kappa)^n}{n!} (\hat{a}_s^\dagger \hat{a}_i^\dagger)^n |N_s, 0_i\rangle \quad (34)$$

or, in case of a degenerate amplifier (in the special cases  $N_s=0\vee 1$ )

$$e^{-i\hat{H}_{\text{deg}} t/\hbar} |N_s\rangle = \cosh^{\frac{(1+2N_s)}{2} 2\kappa} \\ \times \sum_{n=0}^{\infty} \frac{((i/2)e^{i\Delta\theta} \tanh 2\kappa)^n}{n!} (\hat{a}_s^\dagger \hat{a}_s^\dagger)^n |N_s\rangle \quad (35)$$

where  $N_s$  is the number of signal photons initially present, and  $\kappa \equiv \chi t$ . Applying this relation to  $|\psi\rangle_2$ , we obtain the state after the TWPAs.

This equation reproduces the interference visibilities as presented in Figure 2 in case the losses are neglected.

#### A4. Output of Numerical Calculations

From our numerical calculations, we obtain the probability distribution of photon number states,  $\Pr(\langle n \rangle_{A,s} = i, \langle n \rangle_{A,i} = j, \langle n \rangle_{B,s} = k, \langle n \rangle_{B,i} = l)$  in detectors A and B ( $i, j, k, l \in [0, N - 1]$ ). Using partial traces, we can compute the statistics and correlations for each of the four modes and between pairs of modes. For example, the number state probability distribution for signal photons in detector B is shown in Figure 8.

In Figure 9, we show the photon number correlations between the input arms of the second hybrid (arms 5 (top) and 8 (bottom)) for amplifications  $\kappa = 0, 0.5$ , and 1. The top row (Figure 9a–c) shows the correlations between the amount of signal photons in both arms. It can be observed that the correlations are symmetric around the line  $n_{5s} = n_{8s}$ . The second row (Figure 9d–f) shows the correlations between the number of signal and idler photons in arm 5. As shown, the number of idler photons is always equal to the number of signal photons or less by 1, as expected. The final row (Figure 9g–i) shows the correlations between the number of idler photons in arms 5 and 8. For increased amplification, these correlations look more and more like the correlations for the signal photons.

#### A5. Definition of Interference Visibility

In the main text, the interference visibility is defined as

$$V_{s(i)} \equiv \frac{\langle n_{B,s(A,i)} \rangle - \langle n_{A,s(B,i)} \rangle}{\langle n_{B,s(A,i)} \rangle + \langle n_{A,s(B,i)} \rangle} \Big|_{\Delta\theta=0} \quad (39)$$

The rationale behind this definition is shown in Figure 10. At  $\Delta\theta = 0$ , we expect the maximum number of signal photons

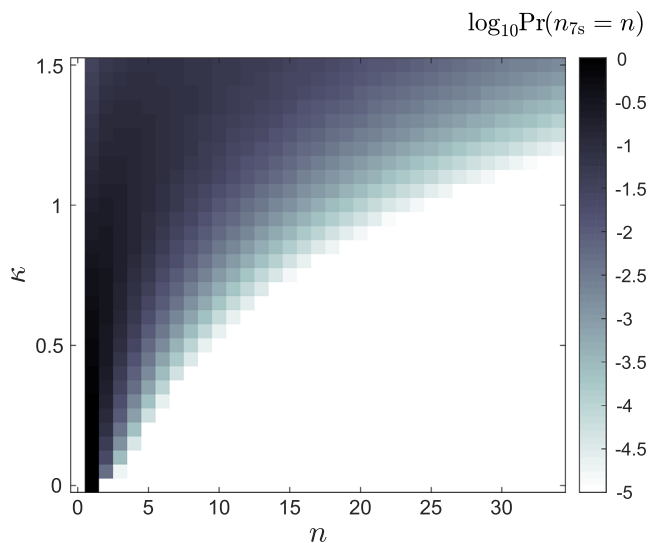


**Figure 8.** Probability distribution of the interferometer's output in arm 7 (detector B) for the signal mode as a function of amplification  $\kappa$ . The probabilities are cutoff at  $\Pr < 10^{-5}$ .

in detector B and the minimum in detector A. For the idler, the opposite is the case.

#### A6. Comparison of Full and Reduced Hilbert Space

As mentioned, the Hilbert space of the full interferometer scales as  $N^4$  (no loss), and the number of entries in the density matrix scales as  $N^8$  (with loss). However, if the amplifiers are identical, we can obtain the same result if we perform the calculation twice—once with a  $|1\rangle_s|0\rangle_i$  input state and once with a  $|0\rangle_s|0\rangle_i$  input state. The first yields  $\langle n_{B,s(A,i)} \rangle$  and the second  $\langle n_{A,s(B,i)} \rangle$ . This implies that the same results can be obtained with a Hilbert space of  $2N^2$  (no loss) or  $2N^4$  (with loss).

In Figure 11, the result of the two calculations is compared as a function of  $\Gamma\Delta t_{\text{TWPA}}$  for  $\kappa = 0.1$  to 0.4. In this figure, the gray solid data correspond to QUTIP's master equation solver, whereas the black dashed data are obtained using the reduced Hilbert space approach. As shown, the results overlap very well, such that we can use the reduced Hilbert space for our calculations.

#### A7. Amplifier Output with Losses

In case transmission losses are considered, we can fit the average number of photons leaving the amplifier with the function

$$\langle n_{s(i)} \rangle_{\text{out}} = \langle n_{s(i)} \rangle_{\text{out}|_{\kappa=0}} \cosh^2 \kappa + (\langle n_{i(s)} \rangle_{\text{out}|_{\kappa=0}} + 1) e^{-f} \sinh^2 \kappa \quad (40)$$

in which  $f$  is a fitting parameter depending on  $\Gamma$ , the various  $\Delta t$  values,  $n_{\text{th}}$  and the input state.

$$\langle n_n \rangle_{\text{out}|_{\kappa=0}} = (\langle n_n \rangle_{\text{in}} - n_{\text{th}}) e^{-\Gamma\Delta t_{\text{tot}}} + n_{\text{th}} \quad (41)$$

is the number of photons of mode  $n$  leaving the amplifier in case the amplification  $\kappa$  equals 0. Here,  $\langle n_n \rangle_{\text{in}}$  is the number of photons of mode  $n$  entering the amplifier.

The result of a particular fit ( $\Gamma = 100$  MHz,  $\Delta t_{\text{TWPA}} = 10$  ns—other  $\Delta t$  values are 1 ns; hence,  $\Gamma\Delta t_{\text{tot}} = 1.3$ ,  $-n_{\text{th}} = 8.3 \times 10^{-3}$ ) is presented in Figure 12. In Figure 13, the magnitude of the fitting factor  $f$  is plotted as a function of  $\Gamma\Delta t_{\text{tot}}$  and  $n_{\text{th}}$ . We observe that the agreement between the simulation and the fitting function is excellent.

Equation (40) can be partially understood from comparison with Equation (3) (repeated here for convenience)

$$\langle \hat{n}_{s(i)} \rangle_{\text{out}} = \langle \hat{n}_{s(i)} \rangle_{\text{in}} \cosh^2 \kappa + (\langle \hat{n}_{i(s)} \rangle_{\text{in}} + 1) \sinh^2 \kappa \quad (42)$$

It is obvious that, for  $\kappa = 0$ ,  $\langle \hat{n}_n \rangle_{\text{in}}$  needs to be replaced by  $\langle n_n \rangle_{\text{out}|_{\kappa=0}}$  to obtain the correct result. For  $\kappa \neq 0$ , it was found that this replacement is not sufficient. By trial and error, we found that multiplying the sinh term with a constant allows us to describe the output correctly. We factor this constant as  $e^{-f}$  in accordance with transmission losses being generally associated with a negative-exponent exponential function. We stress that, although Equation (40) can be used to fit the number of photons leaving the amplifier in the presence of losses, it is not necessarily physically correct. However, for now, we leave

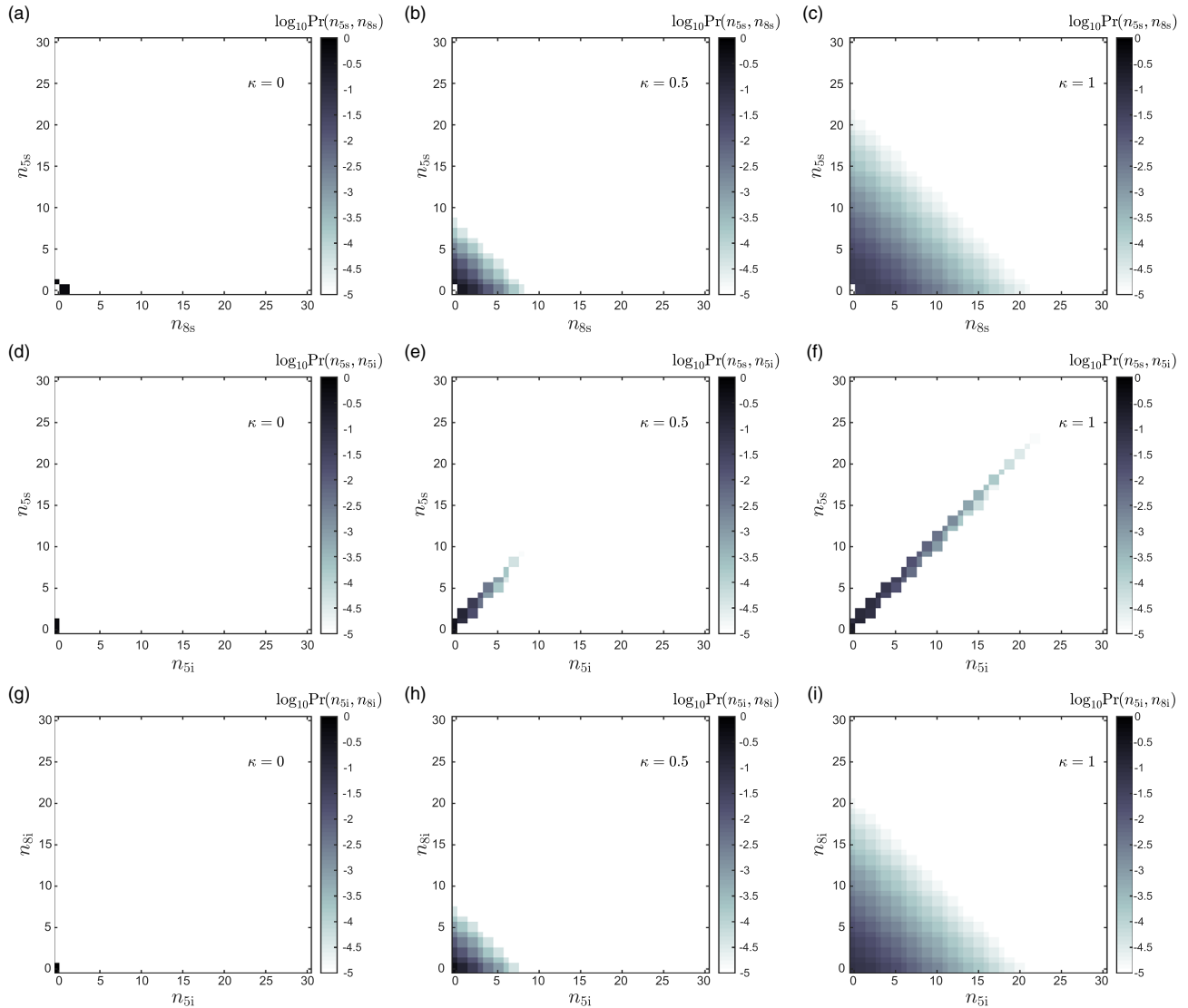


**Figure 9.** Photon number correlations just before the second hybrid for various amplifications  $\kappa$ . a–c) Correlations between number of signal photons in arms 5 and 8. d–f) Correlations between the number of signal photons and idler photons in arm 5. g–i) Correlations between the number of idler photons in arms 5 and 8. The color bars are cutoff at  $\text{Pr} < 10^{-5}$ .

this matter for future consideration, hoping it may help in a future derivation of an expression in a closed form.

#### A8. Interference Visibility with Collapse onto Coherent States

To study the interference visibility in case of state collapse within the interferometer, we assume that the state collapses into a coherent state, the most classical state available in quantum mechanics. Coherent states are expanded in Fock space as

$$|\alpha\rangle = e^{-|\alpha|^2/2} \sum_{n=0}^{\infty} \frac{\alpha^n}{\sqrt{n!}} |n\rangle \quad (43)$$

in which  $\alpha \in \mathbb{C}$  is the amplitude of the coherent state, and  $|n\rangle$  are the number states. The mean number of photons in a coherent state equals  $|\alpha|^2$ . From Equation (43), we can easily compute the overlap between a coherent state and a number state as

$$\langle \alpha | n \rangle = e^{-|\alpha|^2/2} \frac{(\alpha^*)^n}{\sqrt{n!}} \quad (44)$$

Assuming that the interferometer is lossless and that the collapse takes place within the interferometer, the squared overlap between the collapsed coherent state  $|\psi\rangle_{\text{coll}} = |\alpha_{\text{up},s}\rangle |\alpha_{\text{up},i}\rangle |\alpha_{\text{low},s}\rangle |\alpha_{\text{low},i}\rangle$  and the instantaneous quantum state, given by Equation (36) with  $\kappa \mapsto \eta\kappa$ , is

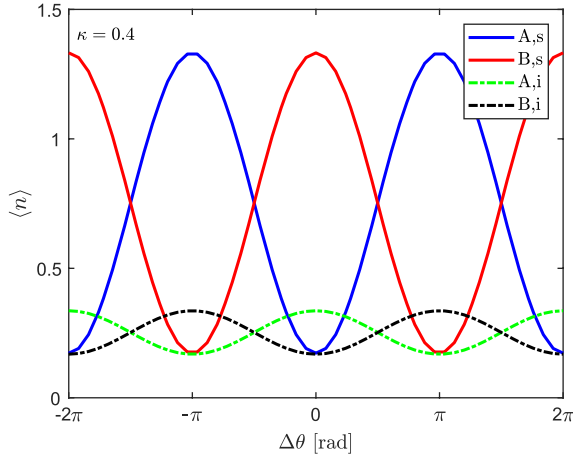


**Figure 10.** Predicted interference pattern of the interferometer in Figure 1 (losses neglected): the average number of signal and idler photons in detectors A and B for amplification 0.4. At phase shift  $\Delta\theta = 0$ , most of the signal photons are expected in detector A, whereas most of the idler photons end up in detector B.

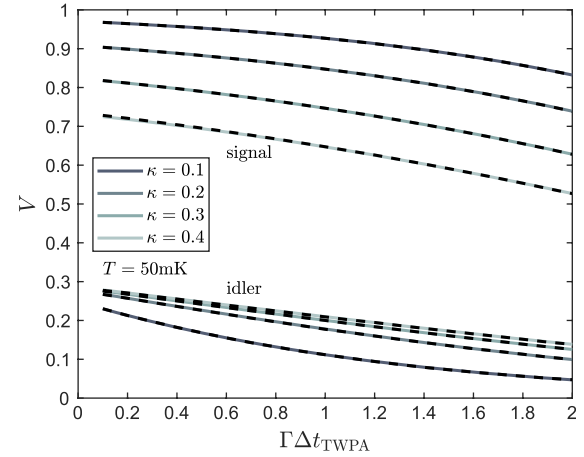


**Figure 11.** Visibility as a function of losses in the TWPA for various  $\kappa$ .  $\Gamma = 100$  MHz,  $T = 50$  mK, and  $\omega_{s,i} = 2\pi \times 5$  GHz.  $\Gamma\Delta t = 0.1$  in the other components of the setup. The data in gray (solid) are obtained from QUTIP's master equation solver using an  $N^6$  Hilbert space with  $N = 5$ . Overlain (black dashed) is the data obtained from the reduced Hilbert space ( $2N^4$ ; see text). As can be observed, the overlap is very good.

$$|c_{\text{coll}}|^2 = |\langle \psi_{\text{coll}} | \psi_3 \rangle|^2 = \frac{e^{-(|\alpha_{\text{up},s}|^2 + |\alpha_{\text{up},i}|^2 + |\alpha_{\text{low},s}|^2 + |\alpha_{\text{low},i}|^2)}}{2 \cosh^6 \eta \kappa} \cdot (|\alpha_{\text{up},s}|^2 + |\alpha_{\text{low},s}|^2 + (i|\alpha_{\text{up},s}| |\alpha_{\text{low},s}| e^{i(\phi_{\text{low},s} - \phi_{\text{up},s})} + \text{c.c.})). \quad (45)$$

$$\cdot \sum_{n,m,l,k} \frac{(i)^{n+m-l-k} \tanh^{n+m+l+k} \eta \kappa}{n!m!l!k!} (|\alpha_{\text{up},s}| |\alpha_{\text{up},i}|)^{n+l} (|\alpha_{\text{low},s}| |\alpha_{\text{low},i}|)^{m+k} \cdot e^{i(n-l)(\phi_{\text{up},s} + \phi_{\text{up},i}) + (m-k)(\phi_{\text{low},s} + \phi_{\text{low},i})}$$

in case the amplifiers are equal and setting the amplitudes to  $\alpha = |\alpha|e^{i\phi_\alpha}$ . The amplifiers evolve the amplitudes of the collapsed state  $|\psi_{\text{coll}}\rangle$  further into average amplitudes

$$\bar{\alpha}_{\text{up(low),s(i)}} = \alpha_{\text{up(low),s(i)}} \cosh(1 - \eta)\kappa + i\alpha_{\text{up(low),i(s)}}^* \sinh(1 - \eta)\kappa \quad (46)$$

and the number of photons arriving in each of the detectors for this particular collapse equals

$$n_{[A]\{B\},n}^{\text{coll}} = \frac{1}{2} |[i]\{1\}\bar{\alpha}_{\text{up},n} + [1]\{i\}\bar{\alpha}_{\text{low},n}|^2 \quad (47)$$

In the last expression, we have used the standard hybrid transformation relations

$$\alpha_{[A]\{B\},n} = \frac{1}{\sqrt{2}} ([i]\{1\}\alpha_{\text{up},n} + [1]\{i\}\alpha_{\text{low},n}) \quad (48)$$

as well as that  $n_{A(B),n}^{\text{coll}} = |\alpha_{A(B),n}|^2$ . Explicitly

$$n_{[A]\{B\},n}^{\text{coll}} = \frac{1}{2} \left[ (|\alpha_{\text{up},s}|^2 + |\alpha_{\text{low},s}|^2) \cosh^2(1 - \eta)\kappa + (|\alpha_{\text{up},i}|^2 + |\alpha_{\text{low},i}|^2) \sinh^2(1 - \eta)\kappa - \right. \\ \left. - (i|\alpha_{\text{up},s}| |\alpha_{\text{up},i}| e^{i(\phi_{\text{up},s} + \phi_{\text{up},i})} \cosh(1 - \eta)\kappa \sinh(1 - \eta)\kappa + \text{c.c.}) + \right. \\ \left. + [1]\{-1\} (i|\alpha_{\text{up},s}| |\alpha_{\text{low},s}| e^{i(\phi_{\text{up},s} - \phi_{\text{low},s})} \cosh^2(1 - \eta)\kappa + \text{c.c.}) + \right. \\ \left. + [1]\{-1\} (|\alpha_{\text{up},s}| |\alpha_{\text{low},i}| e^{i(\phi_{\text{up},s} + \phi_{\text{low},i})} \cosh(1 - \eta)\kappa \sinh(1 - \eta)\kappa + \text{c.c.}) + \right. \\ \left. + [-1]\{1\} (|\alpha_{\text{up},i}| |\alpha_{\text{low},s}| e^{-i(\phi_{\text{up},i} + \phi_{\text{low},s})} \cosh(1 - \eta)\kappa \sinh(1 - \eta)\kappa + \text{c.c.}) + \right. \\ \left. + [1]\{-1\} (i|\alpha_{\text{up},i}| |\alpha_{\text{low},i}| e^{-i(\phi_{\text{up},i} - \phi_{\text{low},i})} \sinh^2(1 - \eta)\kappa + \text{c.c.}) - \right. \\ \left. - (i|\alpha_{\text{low},s}| |\alpha_{\text{low},i}| e^{i(\phi_{\text{low},s} + \phi_{\text{low},i})} \cosh(1 - \eta)\kappa \sinh(1 - \eta)\kappa + \text{c.c.}) \right] \quad (49)$$

$$n_{[A]\{B\},i}^{\text{coll}} = \frac{1}{2} \left[ (|\alpha_{\text{up},s}|^2 + |\alpha_{\text{low},s}|^2) \sinh^2(1-\eta)\kappa + (|\alpha_{\text{up},i}|^2 + |\alpha_{\text{low},i}|^2) \cosh^2(1-\eta)\kappa - (i|\alpha_{\text{up},s}| |\alpha_{\text{up},i}| e^{i(\phi_{\text{up},s} + \phi_{\text{up},i})} \sinh(1-\eta)\kappa \cosh(1-\eta)\kappa + \text{c.c.}) + [1]\{-1\} (i|\alpha_{\text{up},s}| |\alpha_{\text{low},s}| e^{-i(\phi_{\text{up},s} - \phi_{\text{low},s})} \sinh^2(1-\eta)\kappa + \text{c.c.}) + [-1]\{1\} (|\alpha_{\text{up},s}| |\alpha_{\text{low},i}| e^{-i(\phi_{\text{up},s} + \phi_{\text{low},i})} \sinh(1-\eta)\kappa \cosh(1-\eta)\kappa + \text{c.c.}) + [1]\{-1\} (|\alpha_{\text{up},i}| |\alpha_{\text{low},s}| e^{i(\phi_{\text{up},i} + \phi_{\text{low},s})} \sinh(1-\eta)\kappa \cosh(1-\eta)\kappa + \text{c.c.}) + [1]\{-1\} (i|\alpha_{\text{up},i}| |\alpha_{\text{low},i}| e^{i(\phi_{\text{up},i} - \phi_{\text{low},i})} \cosh^2(1-\eta)\kappa + \text{c.c.}) - (i|\alpha_{\text{low},s}| |\alpha_{\text{low},i}| e^{i(\phi_{\text{low},s} + \phi_{\text{low},i})} \sinh(1-\eta)\kappa \cosh(1-\eta)\kappa + \text{c.c.}) \right] \quad (50)$$

With these ingredients, we can obtain the average number of photons arriving in each of the detectors as

$$\langle n_{X,n}^{\text{coll}} \rangle = \frac{1}{\pi^4} \int n_{X,n}^{\text{coll}} |c_{\text{coll}}|^2 d^2\alpha_{\text{up},s} d^2\alpha_{\text{up},i} d^2\alpha_{\text{low},s} d^2\alpha_{\text{low},i} \quad (51)$$

as discussed in the main text. Here,  $d^2\alpha = |\alpha|d\phi_\alpha d\alpha$ , and the bounds of the integrals are  $[0, \infty)$  for integration over the amplitudes and  $[0, 2\pi)$  for integration over the phases.

Due to the complex exponentials in Equation (45) and (49) and the integration over the full domain  $[0, 2\pi)$  for the phases, it is immediately observed that the integrand of Equation (51) only contributes to the integral for integrand terms that are independent of  $\phi_{\text{up}(low),s(i)}$ . Then, integration over the phases yields a factor of  $16\pi^4$ .

For the calculation of  $\langle n_{B,s}^{\text{coll}} \rangle - \langle n_{A,s}^{\text{coll}} \rangle$  and  $\langle n_{A,i}^{\text{coll}} \rangle - \langle n_{B,i}^{\text{coll}} \rangle$ , we find that only the terms scaling as  $e^{\pm i(\phi_{\text{up},s} - \phi_{\text{low},s})}$  and  $e^{\pm i(\phi_{\text{up},i} - \phi_{\text{low},i})}$  from Equation (49) and (50) will contribute to the integral. For the term scaling as  $e^{i(\phi_{\text{up},s} - \phi_{\text{low},s})}$ , we find a contribution to  $\langle n_{B,s}^{\text{coll}} \rangle - \langle n_{A,s}^{\text{coll}} \rangle$

$$\Delta_{s,1} = \frac{8\cosh^2(1-\eta)\kappa}{\cosh^6\eta\kappa} \int |\alpha_{\text{up},s}|^3 |\alpha_{\text{up},i}| |\alpha_{\text{low},s}|^3 |\alpha_{\text{low},i}| \cdot e^{-(|\alpha_{\text{up},s}|^2 + |\alpha_{\text{up},i}|^2 + |\alpha_{\text{low},s}|^2 + |\alpha_{\text{low},i}|^2)} \cdot B_0(2|\alpha_{\text{up},s}| |\alpha_{\text{up},i}| \tanh\eta\kappa) B_0(2|\alpha_{\text{low},s}| |\alpha_{\text{low},i}| \tanh\eta\kappa) \cdot d|\alpha_{\text{up},s}| d|\alpha_{\text{up},i}| d|\alpha_{\text{low},s}| d|\alpha_{\text{low},i}| \quad (52)$$

where we have used the identity  $\sum_{n=0}^{\infty} x^{2n}/(n!)^2 = B_0(2x)$ , in which  $B_n(x)$  is the modified Bessel function of the first kind. For the contribution from Equation (49) scaling as  $e^{-i(\phi_{\text{up},s} - \phi_{\text{low},s})}$ , we find the same expression. For the term in Equation (49) scaling as  $e^{i(\phi_{\text{up},i} - \phi_{\text{low},i})}$ , we find a contribution

$$\Delta_{s,2} = \frac{8\sinh^2(1-\eta)\kappa}{\cosh^6\eta\kappa} \int |\alpha_{\text{up},s}|^2 |\alpha_{\text{up},i}|^2 |\alpha_{\text{low},s}|^2 |\alpha_{\text{low},i}|^2 \cdot e^{-(|\alpha_{\text{up},s}|^2 + |\alpha_{\text{up},i}|^2 + |\alpha_{\text{low},s}|^2 + |\alpha_{\text{low},i}|^2)} \cdot [B_1(2|\alpha_{\text{up},s}| |\alpha_{\text{up},i}| \tanh\eta\kappa) - |\alpha_{\text{up},s}| |\alpha_{\text{up},i}| \tanh\eta\kappa] \cdot [B_1(2|\alpha_{\text{low},s}| |\alpha_{\text{low},i}| \tanh\eta\kappa) - |\alpha_{\text{low},s}| |\alpha_{\text{low},i}| \tanh\eta\kappa] \cdot d|\alpha_{\text{up},s}| d|\alpha_{\text{up},i}| d|\alpha_{\text{low},s}| d|\alpha_{\text{low},i}| \quad (53)$$

to  $\langle n_{B,s}^{\text{coll}} \rangle - \langle n_{A,s}^{\text{coll}} \rangle$ . Here, we have used the identity  $\sum_{n=0}^{\infty} x^{2n+1}/[(n+1)(n!)^2] = B_1(2x) - x$ . Again, the contribution of the term in Equation (49) scaling as  $e^{-i(\phi_{\text{up},i} - \phi_{\text{low},i})}$  yields an equal contribution, such that

$$\langle n_{B,s}^{\text{coll}} \rangle - \langle n_{A,s}^{\text{coll}} \rangle = 2(\Delta_{s,1} + \Delta_{s,2}) \quad (54)$$

For  $\langle n_{A,i}^{\text{coll}} \rangle - \langle n_{B,i}^{\text{coll}} \rangle$ , we find the similar expression

$$\langle n_{A,i}^{\text{coll}} \rangle - \langle n_{B,i}^{\text{coll}} \rangle = 2(\Delta_{i,1} + \Delta_{i,2}) \quad (55)$$

in which  $\Delta_{i,1(2)}$  follow from Equation (52) and (53) by replacing  $\cosh(1-\eta)\kappa$  with  $\sinh(1-\eta)\kappa$  and vice versa.

Similarly, we find that for the calculation of  $\langle n_{B,s}^{\text{coll}} \rangle + \langle n_{A,s}^{\text{coll}} \rangle$  and  $\langle n_{A,i}^{\text{coll}} \rangle + \langle n_{B,i}^{\text{coll}} \rangle$ , only the terms without exponential factor and the terms scaling as  $e^{\pm i(\phi_{\text{up},s} + \phi_{\text{up},i})}$  and  $e^{\pm i(\phi_{\text{low},s} + \phi_{\text{low},i})}$  from Equation (49) and (50) will contribute to the integral. For the terms without exponential, we find a contribution

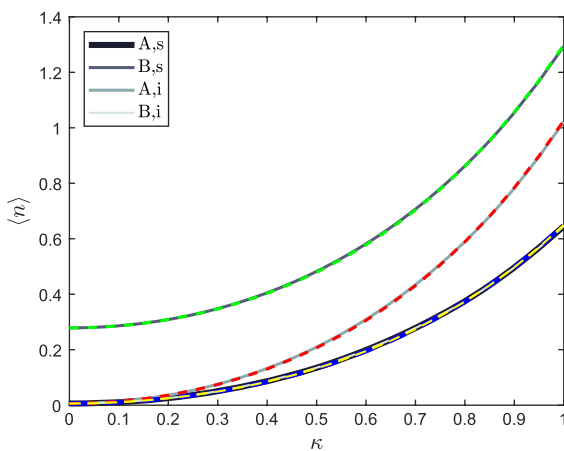


**Figure 12.** Average number of signal and idler photons reaching the detector as a function of  $\kappa$  ( $\Gamma = 100$  MHz,  $\Delta t_{\text{TWPA}} = 10$  ns—other  $\Delta t$  values are 1 ns; hence,  $\Gamma\Delta t_{\text{tot}} = 1.3$ ,  $n_{\text{th}} = 8.3 \times 10^{-3}$ ). The output from the reduced Hilbert space calculation is in gray. The colored dashed lines are the result from a fit using Equation (40). Note that the curves for signal from detector A and idler photons in detector B are overlapping.

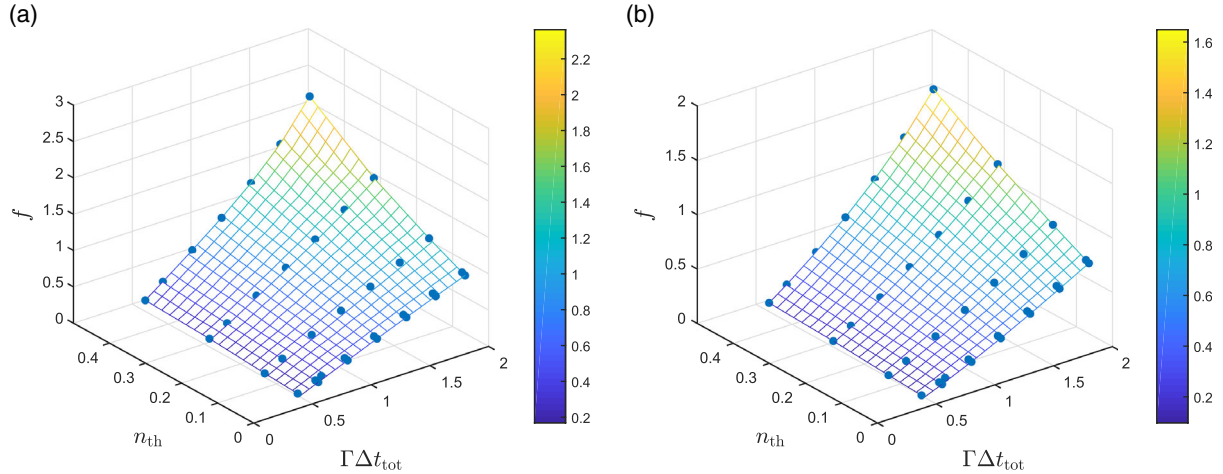


**Figure 13.** Magnitude of the fitting factor  $f$  as a function of  $\Gamma\Delta t_{\text{tot}}$  and  $n_{\text{th}}$  for the case  $\Gamma = 100$  MHz and  $\Delta t_{h_1, ps, h_2} = 1$  ns. a) Should be used for calculating (A,s), (B,s), and (B,i), whereas b) should be used for (A,i). The dots represent the numerical data, whereas the mesh is a linear interpolation.

$$\begin{aligned} \Sigma_{s,1} = & \frac{8}{\cosh^6 \eta \kappa} \int |\alpha_{\text{up},s}| |\alpha_{\text{up},i}| |\alpha_{\text{low},s}| |\alpha_{\text{low},i}| \cdot \\ & \cdot \left[ (|\alpha_{\text{up},s}|^2 + |\alpha_{\text{low},s}|^2) \cosh^2(1 - \eta) \kappa + \right. \\ & \left. + (|\alpha_{\text{up},i}|^2 + |\alpha_{\text{low},i}|^2) \sinh^2(1 - \eta) \kappa \right] \cdot \\ & \cdot (|\alpha_{\text{up},s}|^2 + |\alpha_{\text{low},s}|^2) e^{-(|\alpha_{\text{up},s}|^2 + |\alpha_{\text{up},i}|^2 + |\alpha_{\text{low},s}|^2 + |\alpha_{\text{low},i}|^2)} \cdot \\ & \cdot B_0(2|\alpha_{\text{up},s}| |\alpha_{\text{up},i}| \tanh \eta \kappa) B_0(2|\alpha_{\text{low},s}| |\alpha_{\text{low},i}| \tanh \eta \kappa) \cdot \\ & \cdot d|\alpha_{\text{up},s}| d|\alpha_{\text{up},i}| d|\alpha_{\text{low},s}| d|\alpha_{\text{low},i}| \end{aligned} \quad (56)$$

to  $\langle n_{B,s}^{\text{coll}} \rangle + \langle n_{A,s}^{\text{coll}} \rangle$ . Again, the contribution to  $\langle n_{A,i}^{\text{coll}} \rangle + \langle n_{B,i}^{\text{coll}} \rangle$ ,  $\Sigma_{i,1}$ , is the same except that  $\cosh(1 - \eta) \kappa \mapsto \sinh(1 - \eta) \kappa$ . For the term scaling as  $e^{i(\phi_{\text{up},s} + \phi_{\text{up},i})}$ , we find a contribution

$$\begin{aligned} \Sigma_2 = & \frac{8 \cosh(1 - \eta) \kappa \sinh(1 - \eta) \kappa}{\cosh^6 \eta \kappa} \cdot \\ & \cdot \int |\alpha_{\text{up},s}|^2 |\alpha_{\text{up},i}|^2 |\alpha_{\text{low},s}| |\alpha_{\text{low},i}| (|\alpha_{\text{up},s}|^2 + |\alpha_{\text{low},s}|^2) \cdot \\ & \cdot e^{-(|\alpha_{\text{up},s}|^2 + |\alpha_{\text{up},i}|^2 + |\alpha_{\text{low},s}|^2 + |\alpha_{\text{low},i}|^2)} \cdot \\ & \cdot [B_1(2|\alpha_{\text{up},s}| |\alpha_{\text{up},i}| \tanh \eta \kappa) - |\alpha_{\text{up},s}| |\alpha_{\text{up},i}| \tanh \eta \kappa] \cdot \\ & \cdot B_0(2|\alpha_{\text{low},s}| |\alpha_{\text{low},i}| \tanh \eta \kappa) \cdot \\ & \cdot d|\alpha_{\text{up},s}| d|\alpha_{\text{up},i}| d|\alpha_{\text{low},s}| d|\alpha_{\text{low},i}| \end{aligned} \quad (57)$$

to  $\langle n_{B,s}^{\text{coll}} \rangle + \langle n_{A,s}^{\text{coll}} \rangle$  and  $\langle n_{A,i}^{\text{coll}} \rangle + \langle n_{B,i}^{\text{coll}} \rangle$ . The contribution from the other exponentially scaling terms from Equation (49) and (50) contributing to the integral yields the same values, whence

$$\langle n_{B,s}^{\text{coll}} \rangle + \langle n_{A,s}^{\text{coll}} \rangle = \Sigma_{s,1} + 4\Sigma_2 \quad (58)$$

$$\langle n_{A,i}^{\text{coll}} \rangle + \langle n_{B,i}^{\text{coll}} \rangle = \Sigma_{i,1} + 4\Sigma_2 \quad (59)$$

Using Equation (54), (58), (55), and (59), we easily compute the interference visibilities for signal and idler. We evaluated the integrals in these equations using MATHEMATICA.

## Acknowledgements

The authors would like to thank M.J.A. de Dood for fruitful discussions and C.W.J. Beenakker for the use of the computer cluster. They thank M. de Wit for proofreading this manuscript. They also express their gratitude to the Frontiers of Nanoscience program, supported by the Netherlands Organization for Scientific Research (NWO/OCW), for financial support.

## Conflict of Interest

The authors declare no conflict of interest.

## Keywords

microwave parametric amplifiers, quantum foundations, quantum-to-classical transition, superconducting devices

Received: November 20, 2020  
Published online: December 17, 2020

- [1] X. Gu, A. Kockum, A. Miranowicz, Y. Liu, F. Nori, *Phys. Rep.* **2017**, 718–719, 1.
- [2] A. A. Houck, D. I. Schuster, J. M. Gambetta, J. A. Schreier, B. R. Johnson, J. M. Chow, L. Frunzio, J. Majer, M. H. Devoret, S. M. Girvin, R. J. Schoelkopf, *Nature* **2007**, 449, 328.
- [3] M. Castellanos-Beltran, K. Lehnert, *Appl. Phys. Lett.* **2007**, 91, 083509.
- [4] N. Bergeal, F. Schackert, M. Metcalfe, R. Vijay, V. Manucharyan, L. Frunzio, D. Prober, R. Schoelkopf, S. Girvin, M. Devoret, *Nature* **2010**, 465, 64.
- [5] N. Roch, E. Flurin, F. Nguyen, P. Morfin, P. Campagne-Ibarcq, M. Devoret, B. Huard, *Phys. Rev. Lett.* **2012**, 108, 147701.
- [6] B. Ho Eom, P. Day, H. LeDuc, J. Zmuidzinas, *Nat. Phys.* **2012**, 8, 623.
- [7] C. Eichler, Y. Salathe, J. Mlynek, S. Schmidt, A. Wallraff, *Phys. Rev. Lett.* **2014**, 113, 110502.
- [8] T. Roy, S. Kundu, M. Chand, A. Vadiraj, A. Ranadive, N. Nehra, M. Patankar, J. Aumentado, A. Clerk, R. Vijay, *Appl. Phys. Lett.* **2015**, 107, 262601.
- [9] C. Macklin, K. O'Brien, D. Hover, M. E. Schwartz, V. Bolkhovsky, X. Zhang, W. D. Oliver, I. Siddiqi, *Science* **2015**, 350, 307.

- [10] M. Vissers, R. Erickson, H.-S. Ku, L. Vale, X. Wu, G. Hilton, D. Pappas, *Appl. Phys. Lett.* **2016**, *108*, 012601.
- [11] A. Adamyan, S. de Graaf, S. Kubatkin, A. Danilov, *J. Appl. Phys.* **2016**, *119*, 083901.
- [12] W. H. Louisell, A. Yariv, A. E. Siegman, *Phys. Rev.* **1961**, *124*, 1646.
- [13] T. H. A. van der Reep, arXiv:1812.05907, **2018**.
- [14] P. G. Kwiat, K. Mattle, H. Weinfurter, A. Zeilinger, A. V. Sergienko, Y. Shih, *Phys. Rev. Lett.* **1995**, *75*, 4337.
- [15] C. Vitelli, N. Spagnolo, L. Toffoli, F. Sciarrino, F. De Martini, *Phys. Rev. A* **2010**, *81*, 032123.
- [16] N. Bruno, A. Martin, P. Sekatski, N. Sangouard, R. T. Thew, N. Gisin, *Nat. Phys.* **2013**, *9*, 545.
- [17] B. Hacker, S. Welte, S. Daiss, A. Shaukat, S. Ritter, L. Li, G. Rempe, *Nat. Photon.* **2019**, *13*, 110.
- [18] A. Bassi, K. Lochan, S. Satin, T. P. Singh, H. Ulbricht, *Rev. Mod. Phys.* **2013**, *85*, 471.
- [19] J. R. Johansson, P. D. Nation, F. Nori, *Comput. Phys. Commun.* **2013**, *184*, 1234.
- [20] D. I. Schuster, A. A. Houck, J. A. Schreier, A. Wallraff, J. M. Gambetta, A. Blais, L. Frunzio, J. Majer, B. Johnson, M. H. Devoret, S. M. Girvin, R. J. Schoelkopf, *Nature* **2007**, *445*, 515.
- [21] Y.-F. Chen, D. Hover, S. Sendelbach, L. Maurer, S. T. Merkel, E. J. Pritchett, F. K. Wilhelm, R. McDermott, *Phys. Rev. Lett.* **2011**, *107*, 217401.
- [22] K. Inomata, Z. Lin, K. Koshino, W. D. Oliver, J.-S. Tsai, T. Yamamoto, Y. Nakamura, *Nat. Commun.* **2016**, *7*, 12303.
- [23] L. Rademaker, T. van der Reep, N. Van den Broeck, B. van Waarde, M. de Voogd, T. Oosterkamp, arXiv:1410.2303, **2014**.
- [24] H. P. Breuer, F. Petruccione, *The Theory of Open Quantum Systems*, Oxford University Press, New York **2002**, p. 122.
- [25] K. O'Brien, C. Macklin, I. Siddiqi, X. Zhang, *Phys. Rev. Lett.* **2014**, *113*, 157001.
- [26] M. Bahrani, M. Paternostro, A. Bassi, H. Ulbricht, *Phys. Rev. Lett.* **2014**, *112*, 210404.
- [27] S. Nimmrichter, K. Hornberger, K. Hammerer, *Phys. Rev. Lett.* **2014**, *113*, 020405.
- [28] L. Diósi, *Phys. Rev. Lett.* **2015**, *114*, 050403.
- [29] A. Vinante, M. Bahrani, A. Bassi, O. Usenko, G. Wijts, T. H. Oosterkamp, *Phys. Rev. Lett.* **2016**, *116*, 090402.
- [30] A. Vinante, R. Mezzena, P. Falferi, M. Carlesso, A. Bassi, *Phys. Rev. Lett.* **2017**, *119*, 110401.
- [31] S. M. Barnett, P. M. Radmore, *Methods In Theoretical Quantum Optics*, Oxford University Press, New York **2002**, p. 67.